ELSEVIER

J. Non-Newtonian Fluid Mech. 128 (2005) 71–82

Journal of Non-Newtonian Fluid Mechanics

www.elsevier.com/locate/jnnfm

Numerical investigation of the rheology of a dilute emulsion of drops in an oscillating extensional flow

Xiaoyi Li, Kausik Sarkar *

Department of Mechanical Engineering, University of Delaware, Newark, DE 19716, USA

Received 11 August 2004; received in revised form 25 February 2005; accepted 25 April 2005

Abstract

The rheology of a dilute emulsion of viscous drops in an oscillating extensional flow is investigated. Deforming drop shape is computed using a front tracking finite difference method. Excess stresses due to drops are determined using Bachelor's formula neglecting drop–drop interactions. We present and discuss the relations between the excess stress and the applied strain rate. We explore the linear extensional rheology by computing extensional storage and loss moduli. The effects of frequency and surface tension variations are discussed and compared with analytical models of Oldroyd and Yu and Bousmina. We find that the nature of the excess interfacial stress depends on the relative magnitudes of the time period of oscillation and the relaxation time of the droplet. The excess stress is predominantly elastic (viscous) if the period is much smaller (larger) than the relaxation time. These phenomena are explained using the detail drop dynamics.
© 2005 Elsevier B.V. All rights reserved.

Keywords: Oscillating extension; Viscoelastic; Loss modulus; Storage modulus; Rheology; Excess stress; Complex modulus; Front tracking

1. Introduction

The immiscible liquid–liquid system in the form of emulsions or blends has important applications in numerous chemical industries. In industrial flows of emulsions, suspended drops undergo continuous change of shape including coalescence and breakup, contributing in turn to time-dependent stresses for the overall flow. The co-evolving morphology and rheological response are the fundamental focus of emulsion research [1]. Till date, most deformation studies have been restricted to steady shear and extension. Rheological response for emulsion has been computed mostly for steady shear with a few exceptions of oscillatory shear [2–5]. However, typical industrial flows are far more complex, with large fluctuations, and spatial variations, that can only be represented numerically. In this paper, we report a numerical investigation of rheology in a time-dependent flow, viz., oscillating planar extensional flow. This flow is realizable in a four-roll mill [6], and can offer important rheolgical insights, as will be seen here.

Taylor [7] performed the pioneering experimental investigation of deforming drops, and developed an analytical theory using Lamb's Stokes solution. The subsequent higher order analytical investigations were restricted to nearly spherical [8–11] or slender [12–14] drop shapes (also see [15] for a review). Doi and Ohta presented a coarse grain theory of stresses in a viscosity matched emulsion [16]. They used a morphological quantity—interface tensor—introduced by Batchelor to compute excess stresses due to interfacial tension at the phase boundary [17–19]. The theory is appropriate for describing arbitrary interfacial morphology. However, due to lack of an internal length scale, it gave erroneous results for emulsion of droplets. Various remedies [20–22] have been suggested assuming spherical and ellipsoidal drop shapes. Using ellipsoidal shape assumption, Maffettone and Minale developed a phenomenological tensor model for shape evolution of drops in arbitrary linear flows [23]. The model has been experimentally validated for moderate drop deformation [24,25]. The connection of the drop morphology with rheology was developed by Jansseune et al. [26,27]. Wetzel and Tucker proposed two exact tensor formulations [28,29] for the affine deformation of ellipsoidal drops. They noted that in a linear flow field, the drop shape is exactly ellipsoidal

* Corresponding author. Tel.: +1 302 831 0149; fax: +1 302 831 3619.
E-mail address: sarkar@me.udel.edu (K. Sarkar).

0377-0257/$ – see front matter © 2005 Elsevier B.V. All rights reserved.
doi:10.1016/j.jnnfm.2005.04.001

in the absence of interfacial tension. The theory was extended to approximately account for finite interfacial tension using both small-deformation and slender-body analysis [30]. Wu et al. [31] and Yu and Bousmina [32] combined the ellipsoidal drop models with boundary integrals in order to find a more accurate surface velocity or velocity gradient.

Numerical simulations eliminate any restriction on drop shapes. Large deformation with non-ellipsoidal shape can be treated without using any approximation. Boundary element method (BEM) has been used to study arbitrary deformation including breakup [33,34] and strongly interacting drops in concentrated emulsions [35,36] in a Stokes flow. The flow at finite Reynolds number are computed by a number of direct numerical simulations (DNS) such as volume of fluid (VOF) [37], level set method (LSM) [38] and front tracking method [39]. With advancing computing power, DNS is becoming a viable tool for simulation of multi-drop morphology, and direct computation of rheological response.

Sarkar and Schowalter [40,41] applied front tracking DNS to simulate deformation of a two-dimensional viscous drop in time-periodic extensional flows. The method was extended to viscoelastic drops [42]. Three-dimensional drop deformation in an oscillating extensional flow at finite Reynolds number has recently been computed [43], exploring drop behaviors in detail. In this paper, we use the same simulation technique at a Reynolds number, $Re = 0.1$ (as a representative of Stokes flow; the code can handle only non-zero Reynolds number cases) to obtain the rheological response of a dilute emulation in an oscillating extensional flow. Both drop and continuous phases are Newtonian. For brevity, we present results only for viscosity matched cases, and concentrate on the non-Newtonian response of the emulsion due to the presence of interfacial tension.

In the following, mathematical formulation of the drop problem and its numerical implementation are briefly discussed in Section 2. The expressions for stresses and moduli in oscillating extensional flow are developed in Section 3. In Section 4, we discuss our simulation results. A systematic study of the oscillating stress and its relations with the imposed strain rate, i.e., the loss and storage moduli, is presented. Effects of flow frequency and interfacial tension on the excess stress are investigated. We also present a comparison with the moduli computed by Oldroyd [44,45] and Yu and Bousmina [4]. Finally, Section 5 summarizes the results.

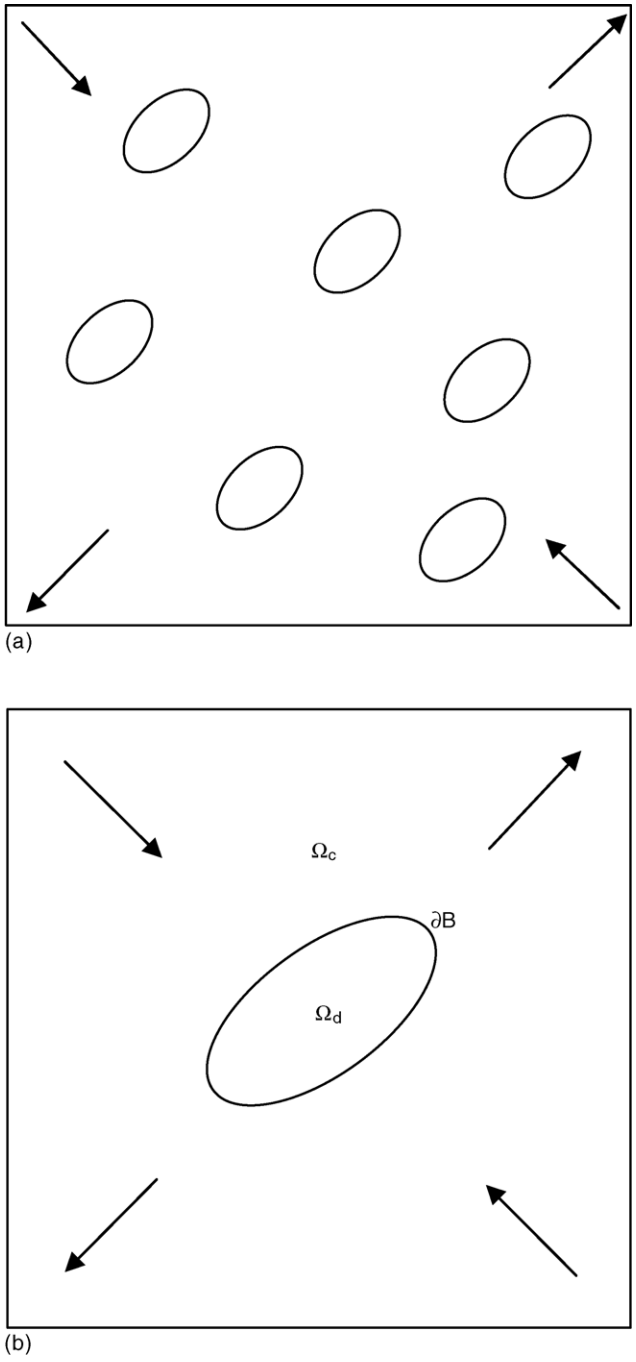

Fig. 1. Schematic of (a) a dilute emulsion in an oscillatory extensional flow and (b) the two-phase Navier–Stokes formalism.

2. Mathematical formulation and numerical implementation of the flow

2.1. Planar oscillating extensional flow

We study flow of an emulsion in a planar oscillating extension:

$$\begin{pmatrix} u \\ v \\ w \end{pmatrix} = \dot{\varepsilon}_0 \cos(\omega t) \begin{pmatrix} 0 & 1 & 0 \\ 1 & 0 & 0 \\ 0 & 0 & 0 \end{pmatrix} \begin{pmatrix} x \\ y \\ z \end{pmatrix}, \quad (1)$$

where $\dot{\varepsilon}_0$ is the amplitude of the strain rate; and ω, the frequency of oscillation. The flow can be generated by an oscillating four-roll mill (Fig. 1a). The dispersed droplets in such a flow experience identical straining. Also note that although the forcing flow is restricted in the x–y plane, the presence of droplets induces fluid motion and excess stress in the z-direction, giving rise to a three-dimensional problem.

2.2. Governing equations

The flow of the Newtonian fluids in the entire domain Ω, which consists of the continuous phase Ω_c and the suspended drops Ω_d (Fig. 1b) is governed by the Navier–Stokes equation

$$\frac{\partial(\rho\mathbf{u})}{\partial t} + \nabla\cdot(\rho\mathbf{u}\mathbf{u}) = -\nabla p - \int_{\partial\mathbf{B}} \mathrm{d}\mathbf{x}_\mathbf{B}\kappa\mathbf{n}\Gamma\,\delta(\mathbf{x}-\mathbf{x}_\mathbf{B}) + \nabla\cdot[\mu\{\nabla\mathbf{u}+(\nabla\mathbf{u})^{\mathrm{T}}\}], \quad (2)$$

where p is the pressure; ρ, the density and μ, the viscosity of the fluid. The superscript 'T' represents transpose. $\partial\mathbf{B}$ is the drop–fluid interface consisting of points $\mathbf{x_B}$; Γ, the constant interfacial tension; κ, the local curvature; $\mathbf{n}$, the outward normal to the interface; and $\delta(\mathbf{x}-\mathbf{x_B})$, the three-dimensional Dirac delta function. The interfacial tension, which produces a jump in the normal stress across the interface, is represented as a singular body force [39,40]. The variation of interfacial tension Γ, e.g., due to presence of surfactant concentration gradient is not considered. The evolution of interface $\mathbf{x_B}$ is coupled with the fluid velocity $\mathbf{u}$ by:

$$\frac{\mathrm{d}\mathbf{x_B}}{\mathrm{d}t} = \mathbf{u}(\mathbf{x_B}). \quad (3)$$

The velocity field is incompressible, i.e., $\nabla\cdot\mathbf{u}=0$.

We simulate the time evolution of a single viscous drop in the planar extensional flow (1). For a dilute emulsion, the interactions between different drops can be neglected, and each drop can be assumed to undergo identical shape evolution. Note that the numerical implementation discussed below can simulate strongly interacting multiple-drop systems [39].

2.3. Numerical implementation

The incompressible flow satisfying Eq. (2) is solved by front tracking method [39,40,42]. We simulate the flow in a finite computational domain, a cubic box of size L. At its boundary, the planar extensional flow (1) is imposed. The method treats the entire flow system as a single phase with material properties varying sharply in a thin region (a few grid points) across the interface. The stress due to surface tension is treated as a distributed force over the same thin region by using a smooth representation of the Dirac delta function in Eq. (2). Here, we provide only a brief description (see [40,43] for further details). The method uses a 3D staggered grid in the entire domain and a triangular grid (Fig. 2) that discretizes the drop surface (front). Using the front position, a smoothed description of the material property is obtained. It reduces the multiphase flow into a single phase with varying properties. The single phase flow is then solved by an operator splitting/projection finite difference method. In the first step, an intermediate velocity is obtained using all terms in (2) except the pressure gradient. The intermediate velocity is then corrected using pressure gradient so that the final velocity satisfies divergence condition. The pressure gradient correction

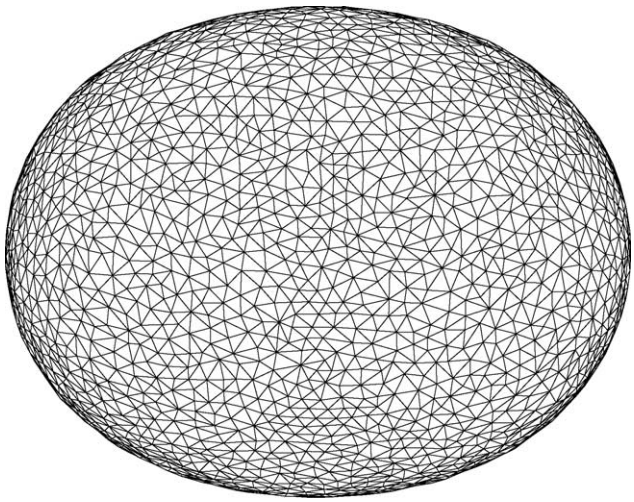

Fig. 2. Drop surface discretized by triangular elements.

obtains a Poisson equation which is solved using a multigrid method. The velocity at the 3D grid is interpolated to front nodes, and the front is updated to obtain its new position. To prevent the front element from being excessively distorted, an adaptive regridding scheme is implemented for the front. The explicit scheme is inherently limited to finite Reynolds number, and suffers from severe diffusion limited restrictions on time steps at low Reynolds numbers. We use $Re = 0.1$ for all our computation as a representative case for low Reynolds number. To overcome the time step restriction, we treat the diffusive terms semi-implicitly in alternate spatial directions (ADI). ADI enhances the efficiency of the simulation by one order of magnitude.

2.4. Non-dimensional parameters

The mathematical problem can be non-dimensionalized using undeformed drop radius R and inverse extensional rate $\dot{\varepsilon}_0^{-1}$ as the length and the time scales, respectively. We obtain five non-dimensional parameters—Reynolds number, $Re = \rho\dot{\varepsilon}_0 R^2/\mu$; inverse capillary number, $k = Ca^{-1} = \Gamma/(\dot{\varepsilon}_0\mu R)$; viscosity ratio, $\lambda = \mu_d/\mu$; density ratio, $\lambda_\rho = \rho_d/\rho$ and the non-dimensional frequency Strouhal number, $St = \omega/\dot{\varepsilon}_0$. The subscript 'd' represents the drop phase. As already mentioned, we restrict the simulation to $Re = 0.1$ (see [43] for effects of Reynolds number variation on drop deformation). For brevity, we consider a viscosity and density matched emulsion, resulting in only an interfacial contribution to the excess stress. Note that the numerical scheme introduced above can handle non-uniform material properties.

3. Interfacial stress and extensional moduli

3.1. Interfacial stress averaging

An emulsion can be viewed as a statistically indeterminate collection of droplets in a continuous phase [17]. The

stress measured in experiments is an average over an ensemble of realizations. It is equivalent to a volume average with an appropriate volume chosen to satisfy the condition of statistical stationarity and homogeneity. The averaging procedure was introduced by Batchelor and extensively deployed in suspensions [18,22]. As pointed out by Jansseune et al. [26,27], the average stress can be divided into two contributions, one from the component fluids and the other from the interface.

For both dispersed and the continuous phases satisfying Newtonian constitutive relation, the averaged stress $\boldsymbol{\sigma}_{\text{ave}}$ can be expressed as [1,17–19]:

$$\begin{aligned}\boldsymbol{\sigma}_{\text{ave}} &= \frac{1}{V}\int_V \boldsymbol{\sigma}\,\mathrm{d}V \\ &= -P_{\text{ave}}\mathbf{I} + \boldsymbol{\tau}_{\text{ave}} + \frac{\mu_{\text{d}}-\mu}{V}\sum\int_{A_{\text{d}}}(\mathbf{un}+\mathbf{nu})\,\mathrm{d}A \\ &\quad -\Gamma\mathbf{q}, \end{aligned} \tag{4}$$

where V is the averaging volume, V_{d} and A_{d} are the volume and surface area of a typical drop. P_{ave} is the isotropic part of the average stress; $\mathbf{I}$, the identity tensor, and $\boldsymbol{\tau}_{\text{ave}}$ is the deviatoric part of the average "component" stress [26,34]. The third term is the contribution due to viscosity difference between the drop and the continuous phases. It becomes zero for $\lambda = 1$. The fourth term is the excess stress representing the contribution of the interfacial morphology:

$$\boldsymbol{\sigma}_{\text{excess}} = -\Gamma\mathbf{q}, \qquad \mathbf{q} = \frac{1}{V}\sum\int_{A_{\text{d}}}\left(\mathbf{nn}-\frac{\mathbf{I}}{3}\right)\mathrm{d}A. \tag{5}$$

where $\mathbf{q}$ is the anisotropy or interface tensor [1,16], is a purely geometric quantity; $\mathbf{n}$, as before is the outward unit normal vector at the drop interface; and $\partial\mathbf{B}$ consists of all drop–fluid interfaces. The interface tensor is calculated by numerical integration over the discretized interface (Fig. 2).

For a dilute emulsion consisting of m identical droplets with volume V_{d} and surface area A_{d} in the averaging volume V, the interface tensor can be expressed as a sum of individual drop contributions:

$$\mathbf{q} = \Phi\mathbf{q}_{\text{d}}, \qquad \mathbf{q}_{\text{d}} = \frac{1}{V_{\text{d}}}\int_{A_{\text{d}}}\left(\mathbf{nn}-\frac{\mathbf{I}}{3}\right)\mathrm{d}A, \tag{6}$$

where $\Phi = mV_{\text{d}}/V$ is the volume fraction of drops. The excess stress $\boldsymbol{\sigma}_{\text{excess}}$ non-dimensioanlized by $\mu\dot{\varepsilon}_0$ is

$$\begin{aligned}\sum\nolimits_{\text{excess}} &\equiv \frac{\boldsymbol{\sigma}_{\text{excess}}}{\mu\dot{\varepsilon}_0} = \Phi\sum\nolimits^{\text{d}}_{\text{excess}}, \\ \sum\nolimits^{\text{d}}_{\text{excess}} &= -\frac{\Gamma}{\mu\dot{\varepsilon}_0}\mathbf{q}_{\text{d}} = -kR\mathbf{q}_{\text{d}}. \end{aligned} \tag{7}$$

Note that as expected in this non-interacting dilute system, the stress is linear with volume fraction. The single-drop non-dimensionalized excess stress $\sum^{\text{d}}_{\text{excess}}$ depends only on the drop shape and is computed from the numerical simulation.

3.2. Interfacial extensional moduli

From one-drop excess stress and its phase relation with the imposed flow strain, the complex moduli can be calculated. Taking the coordinate axes along the axes of extension [clockwise rotated by $\pi/4$ from the x–y axes of Eq. (1)], we obtain the principal directions for the excess stress. It takes diagonal form due to the symmetry of drop shape:

$$\sum\nolimits^{\text{d}}_{\text{excess}} = \begin{pmatrix} \sum^{\text{d}}_{11} & 0 & 0 \\ 0 & \sum^{\text{d}}_{22} & 0 \\ 0 & 0 & \sum^{\text{d}}_{33} \end{pmatrix} \tag{8}$$

The oscillating extensional flow (1) in diagonal form gives rise to equal positive and negative strains along the extensional axes:

$$\varepsilon = \int\dot{\varepsilon}\,\mathrm{d}t = \frac{\dot{\varepsilon}_0}{\omega}\sin\omega t = \frac{1}{St}\sin(t'St), \tag{9}$$

where $t' = t\dot{\varepsilon}_0$ is non-dimensional time and $\varepsilon_0 = \dot{\varepsilon}_0/\omega = 1/St$ is the strain amplitude. We consider the non-dimensional normal stress difference, $\sum^{\text{d}}_{22} - \sum^{\text{d}}_{11}$. Denoting the phase difference between $\sum^{\text{d}}_{22} - \sum^{\text{d}}_{11}$ and the imposed flow strain as δ, we have:

$$\sum\nolimits^{\text{d}}_{22} - \sum\nolimits^{\text{d}}_{11} = \left(\sum\nolimits^{\text{d}}_{22} - \sum\nolimits^{\text{d}}_{11}\right)^0 \sin(t'St+\delta), \tag{10}$$

where superscript '0' represents amplitude. Therefore, by examining the in-phase and the out-of-phase parts of $\sum^{\text{d}}_{22} - \sum^{\text{d}}_{11}$, we obtain non-dimensional storage and loss moduli, respectively:

$$\begin{aligned} E^{\text{d}'}_{\text{int}} &= \left(\sum\nolimits^{\text{d}}_{22} - \sum\nolimits^{\text{d}}_{11}\right)^0 St\cos\delta, \\ E^{\text{d}''}_{\text{int}} &= \left(\sum\nolimits^{\text{d}}_{22} - \sum\nolimits^{\text{d}}_{11}\right)^0 St\sin\delta. \end{aligned} \tag{11}$$

Using Eqs. (7), (8) and (11), we compute the extensional moduli for various flow parameters such as frequencies (St) and interfacial tension (k).

3.3. Oldroyd's and Yu and Bousmina's model

Oldroyd [44,45] derived analytical expressions for linear viscoelasticity of a dilute Newtonian emulsion using an asymptotic approach. He obtained Jeffrey's equation:

$$\boldsymbol{\sigma} + \tau_1\frac{\mathrm{d}}{\mathrm{d}t}\boldsymbol{\sigma} = 2\mu_0\left(\dot{\boldsymbol{\varepsilon}} + \tau_2\frac{\mathrm{d}}{\mathrm{d}t}\dot{\boldsymbol{\varepsilon}}\right) \tag{12}$$

with

$$\begin{aligned} &\mu_0 = \mu(1+A_1\Phi), \quad \tau_1 = \tau_0(1+A_2\Phi), \\ &\tau_2 = \tau_0(1-A_3\Phi), \\ &A_1 = \frac{(5\lambda+2)}{[2(\lambda+1)]}, \quad A_2 = \frac{(19\lambda+16)}{[5(\lambda+1)(2\lambda+3)]}, \\ &A_3 = \frac{3(19\lambda+16)}{[10(\lambda+1)(2\lambda+3)]}, \quad \tau_0 = \frac{(19\lambda+16)(2\lambda+3)\mu R}{[40\Gamma(\lambda+1)]} \end{aligned} \tag{13}$$

For oscillating flows, assuming periodic variation for the stress $\boldsymbol{\sigma} = \boldsymbol{\sigma}_0 \exp(i\omega t)$ and the strain rate $\dot{\boldsymbol{\epsilon}} = \dot{\boldsymbol{\epsilon}}_0 \exp(i\omega t)$, we obtain from Eq. (12):

$$(1 + i\omega\tau_1)\boldsymbol{\sigma} = 2\mu_0(1 + i\omega\tau_2)\dot{\boldsymbol{\epsilon}} \tag{14}$$

In a planar extensional flow along the principal direction

$$\dot{\boldsymbol{\epsilon}} = \dot{\varepsilon}_0 \begin{pmatrix} 1 & 0 & 0 \\ 0 & -1 & 0 \\ 0 & 0 & 0 \end{pmatrix}$$

noting $\varepsilon = \int \dot{\varepsilon}\, \mathrm{d}t = \dot{\varepsilon}/i\omega$, the complex extensional modulus non-dimensionalized by $\mu\dot{\varepsilon}_0$ is:

$$E = \frac{1}{\mu\dot{\varepsilon}_0}\frac{\sigma_{22} - \sigma_{11}}{\varepsilon} = i4St\frac{\mu_0}{\mu}\frac{1 + i\omega\tau_2}{1 + i\omega\tau_1}. \tag{15}$$

Note that the extensional modulus E in a planar extensional flow and the shear modulus G are related by the Trouton ratio: $E = 4G$. Using (13), Eq. (15), after linearization with respect to Φ, becomes:

$$E = i4St[1 + (A_1 - A_2 - A_3)\Phi] + i4St\frac{A_2 + A_3}{1 + \omega^2\tau_0^2}\Phi + 4St\omega\tau_0\frac{A_2 + A_3}{1 + \omega^2\tau_0^2}\Phi. \tag{16}$$

The modulus is further decomposed into a bulk part (independent of interfacial relaxation τ_0) and an interfacial part, each of which consists of a storage modulus (prime) and a loss modulus (double prime):

$$\begin{aligned} &E = E' + iE'' = (E'_{\text{bulk}} + E'_{\text{int}}) + i(E''_{\text{bulk}} + E''_{\text{int}}), \\ &E'_{\text{bulk}} = 0, \quad E''_{\text{bulk}} = 4St[1 + (A_1 - A_2 - A_3)\Phi], \\ &E'_{\text{int}} = 4St\omega\tau_0\frac{A_2 + A_3}{1 + \omega^2\tau_0^2}\Phi, \quad E''_{\text{int}} = 4St\frac{A_2 + A_3}{1 + \omega^2\tau_0^2}\Phi. \end{aligned} \tag{17}$$

Note that the linearization in volume fraction leads to moduli proportional to volume fraction Φ, appropriate for the first order theory of a dilute emulsion. The one-drop moduli are obtained dividing the above expressions by Φ as in Eq. (7).

Recently, Yu and Bousimina [4] presented a model for both linear and nonlinear shear rheology of Newtonian emulsions. For small amplitude oscillatory shear, the interfacial storage and loss shear moduli non-dimensionalized by $\mu\dot{\varepsilon}_0$ are given as (Eqs. (16)–(18) in [4]):

$$G'_{\text{int}} = \frac{B_1\omega^2\tau_0^2}{\mu\dot{\varepsilon}_0(1 + \omega^2\tau_0^2)}, \qquad G''_{\text{int}} = \frac{B_1\omega\tau_0}{\mu\dot{\varepsilon}_0(1 + \omega^2\tau_0^2)}, \tag{18}$$

where

$$B_1 = \frac{20(\lambda + 1)}{(2\lambda + 3)[5(\lambda + 1) - (5\lambda + 2)\Phi]}\frac{\Gamma}{R} \approx \frac{4\Phi}{2\lambda + 3}\frac{\Gamma}{R}, \tag{19}$$

the second step being a linearization in Φ. For viscosity matched drop ($\lambda = 1$), the model predicts:

$$G'_{\text{int}} = \frac{4\omega^2\tau_0^2 k}{5(1 + \omega^2\tau_0^2)}\Phi, \qquad G''_{\text{int}} = \frac{4\omega\tau_0 k}{5(1 + \omega^2\tau_0^2)}\Phi \tag{20}$$

Comparing with the Oldroyd model (17) for $\lambda = 1$, we obtain E (Oldroyld) = $4G$ (Bousmina). In this limit the models are equivalent.

4. Results

We simulate a single viscous drop in a box-shaped domain as shown in Fig. 3, with oscillating extensional flow imposed at the domain boundary. The undeformed drop radius R is one-tenth the domain size L. By varying domain size, we have ensured that the simulation is independent of the size of the domain. We also checked for grid-convergence by increasing the discretization from $81 \times 81 \times 81$ to $129 \times 129 \times 129$ without finding significant change in the result.

4.1. Oscillating droplet morphology

The drop in a linear flow maintains an approximate ellipsoidal shape [24,25]. We plot the three axes of the ellipsoids with non-dimensional time $t' = t\dot{\varepsilon}_0$ in Fig. 4a. The initially spherical drop oscillates with the imposed flow. The maximum (L) and the minimum (B) axes are the maximum and the minimum distances of the drop surface from its center, and they lie in the plane of the extension. The points at the maximum and minimum distances switch when the direction of extension changes in the course of oscillation. The

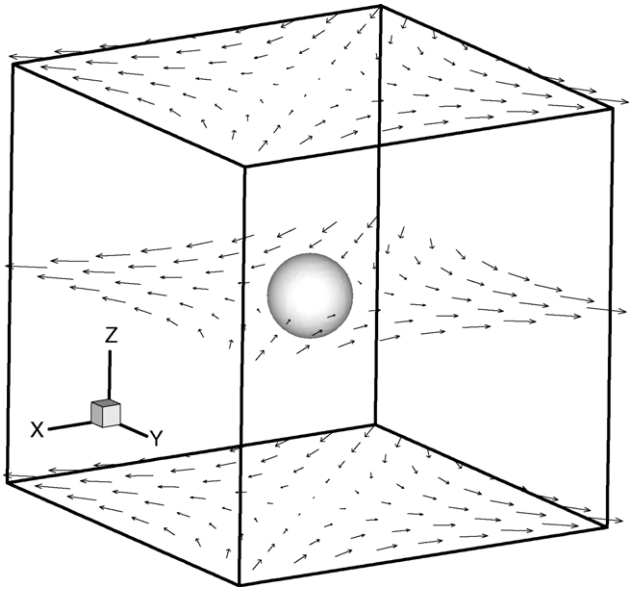

Fig. 3. A spherical drop is initially placed at the center of the domain. An oscillatory extension flow is imposed at the boundary of the domain.

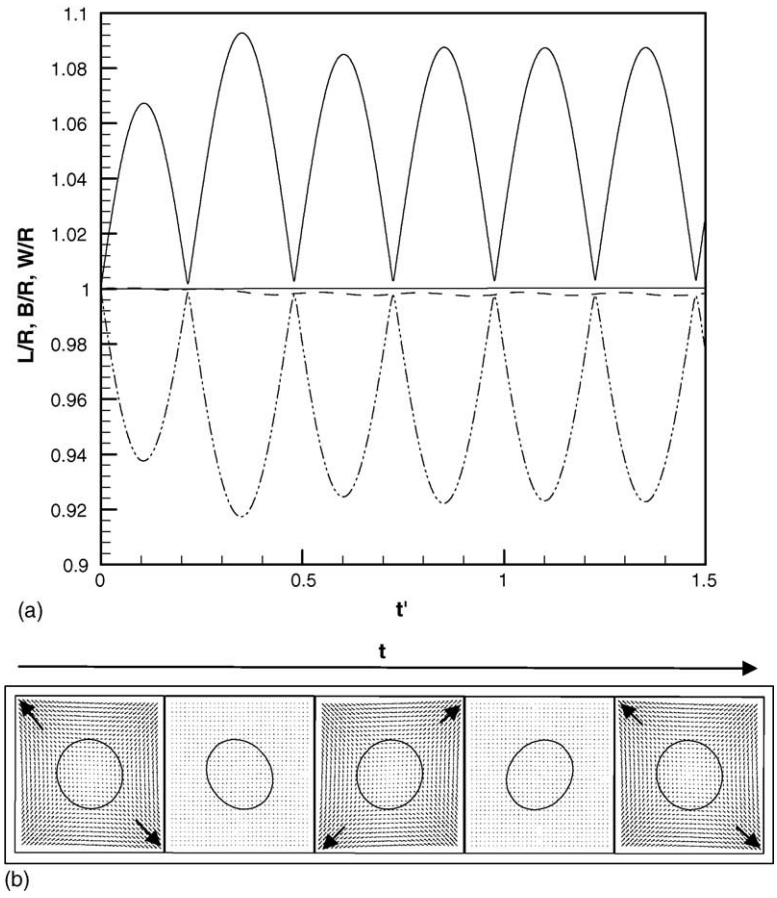

Fig. 4. (a) Drop axes evolving with non-dimensional time in an oscillatory extensional flow; length, L (solid); breadth, B (dash-double-dotted); width, W (dashed). (b) Drop shape in one period in steady state; $Re = 0.1$, $St = 4\pi$, $k = 10$.

width axis W, which is the maximum distance in the direction perpendicular to the plane of extension, does not change much ($W/R \sim 1.0$), indicating that the deformation is small in the direction orthogonal to the plane of the flow. These axes reach a steady-oscillating state following a short transient. The frequency of drop oscillation follows the frequency of the imposed flow. In Fig. 4b, the top view (z-direction) of drop shape in the oscillating flow is shown together with the flow field in a plane through the center of the drop. The drop experiences stretching in alternate orthogonal directions. Within one period of the flow, the deformation reaches maximum twice. The maximum deformation does not coincide with the maximum strain rate (velocity) of the flow (first, third, fifth frames), indicating a finite phase lag in the drop response. As will be seen shortly, the excess stresses, which result from interfacial tension acting at the drop boundary, oscillate similarly with the imposed strain rate.

We study drop deformation using the parameter $D = (L - B)/L + B$, suggested by Taylor [7]. In Fig. 5, we summarize the drop response as a function of non-dimensional frequency St, and interfacial tension k. As we saw in Fig. 4a, the drop performs a steady oscillation following a short transient. In Fig. 5a, the maximum deformation D_{max} and the phase difference β ($=\pi/2 - \delta$) between deformation D and flow strain rate $\dot{\varepsilon}$ are plotted as functions of St, at a constant interfacial tension parameter $k = 45$. At relatively high frequencies ($St > 5\pi$), D_{max} decreases with increasing flow frequency. Increased frequency leads to quick reversals of flow direction so that the drop does not deform appreciably. The slight increase in D_{max} for lower frequencies ($St > 5\pi$) leading to a peak is a resonance effect of the low but finite inertia, explained in detail in [43]. The phase difference β increases from 0 to $\pi/2$ with the increase of flow frequency St. At low frequency $St \to 0$, the deformation is in phase with the strain rate $\dot{\varepsilon}$. As $St \to \infty$, the deformation is $\pi/2$ behind the strain rate $\dot{\varepsilon}$, but in phase with the flow strain ε. In Fig. 5b, we plot the same quantities D_{max} and β with varying interfacial tension parameter k subject to the same flow frequency ($St = 4\pi$). D_{max} displays monotonic decrease with increasing k for $k > 10$. Increased interfacial tension restrains drop deformation. Similar to Fig. 5a, we see a small peak caused by finite inertia at lower values of k. The phase β decreases with increasing k. For extremely high interfacial tension, the deformation is in phase with the strain rate. The drop response is discussed in detail with the help of a simple damped mass-spring model in [43].

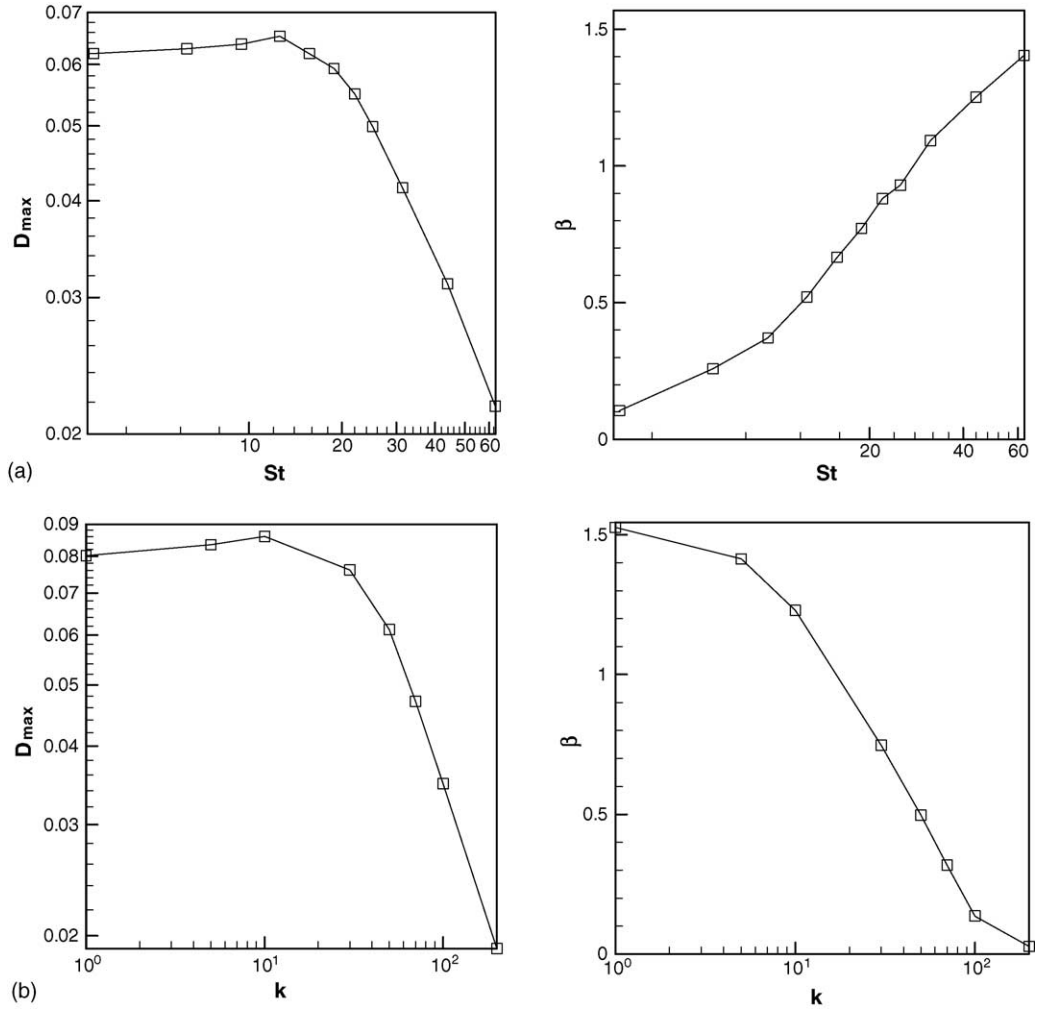

Fig. 5. (a) D_{max} and β vs. St; $Re = 0.1$, $k = 45$; (b) D_{max} and β vs. k; $Re = 0.1$, $St = 4\pi$.

4.2. Excess stress

From the simulated drop shape, we compute one-drop excess non-dimensional stress $\sum^{d}_{excess}$, appropriate for a dilute emulsion. In Fig. 6, we investigate the non-dimensional excess stress difference $\Sigma^{d}_{22} - \Sigma^{d}_{11}$ and its relation to the imposed strain rate $\dot{\varepsilon}/\dot{\varepsilon}_0$. The sinusoidal variation of the strain rate (dashed curve) is plotted at top left. In the subsequent plots, $\Sigma^{d}_{22} - \Sigma^{d}_{11}$ is shown in the steady-oscillation state ($t' > t'_{steady}$) for the same interfacial tension parameter $k = 45$ but different flow frequencies ($St = \pi$, 8π, 20π). The magnitude of the stress difference decreases due to decreased drop deformation with increasing flow frequency (see Fig. 5a). To demonstrate the phase of stress oscillation, the time t' is scaled by $St(t'St = \omega t)$. For drops with moderate interfacial tension $k = 45$, at a low flow frequency $St = \pi$, the resulting excess stress difference $\Sigma^{d}_{22} - \Sigma^{d}_{11}$ is in phase with the strain rate of the flow. However, at a high frequency $St = 20\pi$, $\Sigma^{d}_{22} - \Sigma^{d}_{11}$ lags by $\pi/2$ behind strain rate, with intermediate phase lag for $St = 8\pi$. The stress–strain rate relation indicates that the emulsion behaves as a viscous liquid at low frequencies, and elasticity takes precedence as the frequency increases. The oscillation of stress is closely related to the oscillation of drop deformation. In Fig. 7, the top view of the drop (from z-direction) is shown together with the velocity field in the plane through the center of the drop. For both low ($St = \pi$) and high ($St = 20\pi$) frequencies, the shape of the deformed drop at different time-instants are plotted. At a low frequency $St = \pi$, the drop deforms in phase with the strain rate, the latter represented by velocity vectors. At a high frequency $St = 20\pi$, a phase difference of $\pi/2$ exists between the deformation and the strain rate. As the strain rate achieves maximum (bottom left and right frames), deformation approaches zero. For zero strain rate (bottom middle frame), deformation reaches the maximum.

In Fig. 8, similar curves as those in Fig. 7 are shown. However, drops with different interfacial tension ($k = 1$, 50, 200) are forced by a flow with the same frequency $St = 4\pi$. At low interfacial tension $k = 1$, $\Sigma^{d}_{22} - \Sigma^{d}_{11}$ lags by $\pi/2$ behind the strain rate $\dot{\varepsilon}/\dot{\varepsilon}_0$. At high interfacial tension $k = 200$, $\Sigma^{d}_{22} - \Sigma^{d}_{11}$ is in phase with the strain rate, with a transi-

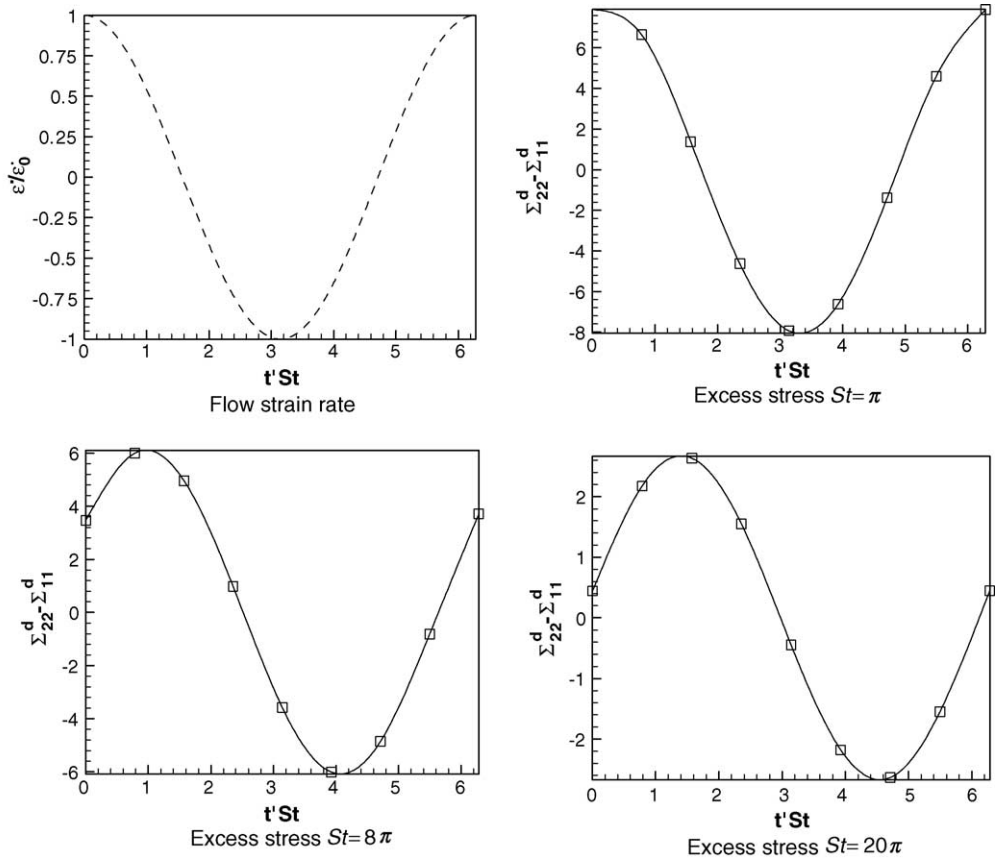

Fig. 6. Variation of flow strain rate (top left) and one-drop excess stress difference $\Sigma_{22}^{\mathrm{d}} - \Sigma_{11}^{\mathrm{d}}$ (others), during one period of steady oscillation; $k = 45$, $Re = 0.1$.

tion at intermediate values of interfacial tension. However, note that for the low value of interfacial tension $k = 1$, the stress is much less than those for the other two cases. In the limit of zero interfacial tension, the excess stress is in phase with the flow strain, characteristic of an elastic material, due to the fact that the drop shape follows the flow strain. The drop deformation rate is in phase with the imposed strain rate, and thereby the drop shape $\pi/2$ behind the strain rate. The excess interfacial stress is proportional to drop deformation. For high interfacial tension, drop is more elastic; its deformation is in phase with the strain rate, giving rise to interfacial stress proportional to imposed strain rate, a viscous behavior. Therefore, when the drop behaves as a viscous system at low interfacial tension, the resulting interfacial stress of the emulsion is elastic, and when the drop behaves like an elastic system at high interfacial tension, the interfacial stress is viscous. Note that we are only concerned here with the excess stress, and not the total stress which includes the stresses due to the component liquids. Even though the excess interfacial stress $\Sigma_{22}^{\mathrm{d}} - \Sigma_{11}^{\mathrm{d}}$ is elastic at low interfacial tension, it vanishes in proportion with the interfacial tension. In the limit of an infinitely large interfacial tension, the excess stress is viscous, because the drop does not deform much. The overall emulsion behavior is viscoelastic for moderate values of interfacial tensions where drop deformation is significant.

4.3. Complex interfacial extensional moduli

We investigate the linear extensional rheology using storage and loss moduli $E_{\mathrm{int}}^{\mathrm{d}'}$ and $E_{\mathrm{int}}^{\mathrm{d}''}$ introduced in Section 3.2. We compare with analytical expressions for moduli obtained by Oldroyd [44,45] (the same as that due to Yu and Bousmina [4]). In Fig. 9a, the variation of the non-dimensional interfacial extensional moduli with frequency St is shown. Our results match very well with analytical prediction. At low flow frequency, the phase difference δ between stress and strain approaches $\pi/2$ ($\delta = \pi/2 - \beta$), so that $E_{\mathrm{int}}^{\mathrm{d}'}$ approaches zero much faster than $E_{\mathrm{int}}^{\mathrm{d}''}$. In this case, viscous dissipation is dominant and the emulsion behaves like a Newtonian fluid. As the imposed flow frequency increases, δ decreases such that the curve of $E_{\mathrm{int}}^{\mathrm{d}'}$ and $E_{\mathrm{int}}^{\mathrm{d}''}$ cross each other. Both viscous dissipation and elasticity are significant rendering the emulsion viscoelastic. At the other end of high flow frequencies, δ approaches zero and $E_{\mathrm{int}}^{\mathrm{d}'}$ is much larger than $E_{\mathrm{int}}^{\mathrm{d}''}$, indicating strong elasticity. In conformity with analytical results (17) and (20), for $St \to \infty$ we find $E_{\mathrm{int}}^{\mathrm{d}'} \to 16k/5 = 144$ and $E_{\mathrm{int}}^{\mathrm{d}''} \to 0$. Our results seem to deviate from the analytical theories at high frequencies ($St = 3\pi$). It is an effect of small but finite inertia. The unsteady term $\partial(\rho u)/\partial t$ in Navier–Stokes Eq. (2) is $\sim O(ReSt)$. At sufficiently high frequency, even for the present case of small $Re = 0.1$, it can become sig-

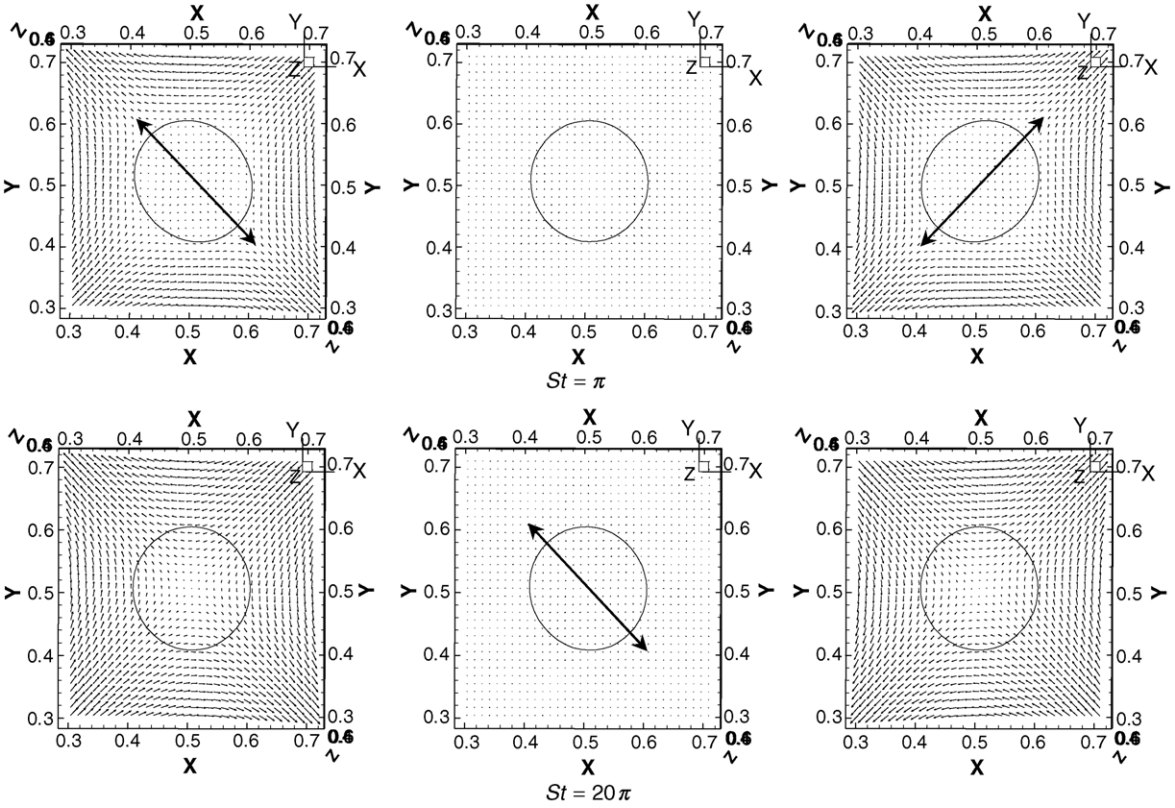

Fig. 7. Top view of the drop from z-direction in the plane through the center of the drop for three different time-instants for $St = \pi$ (top) and $St = 20\pi$ (bottom); $k = 45$, $Re = 0.1$.

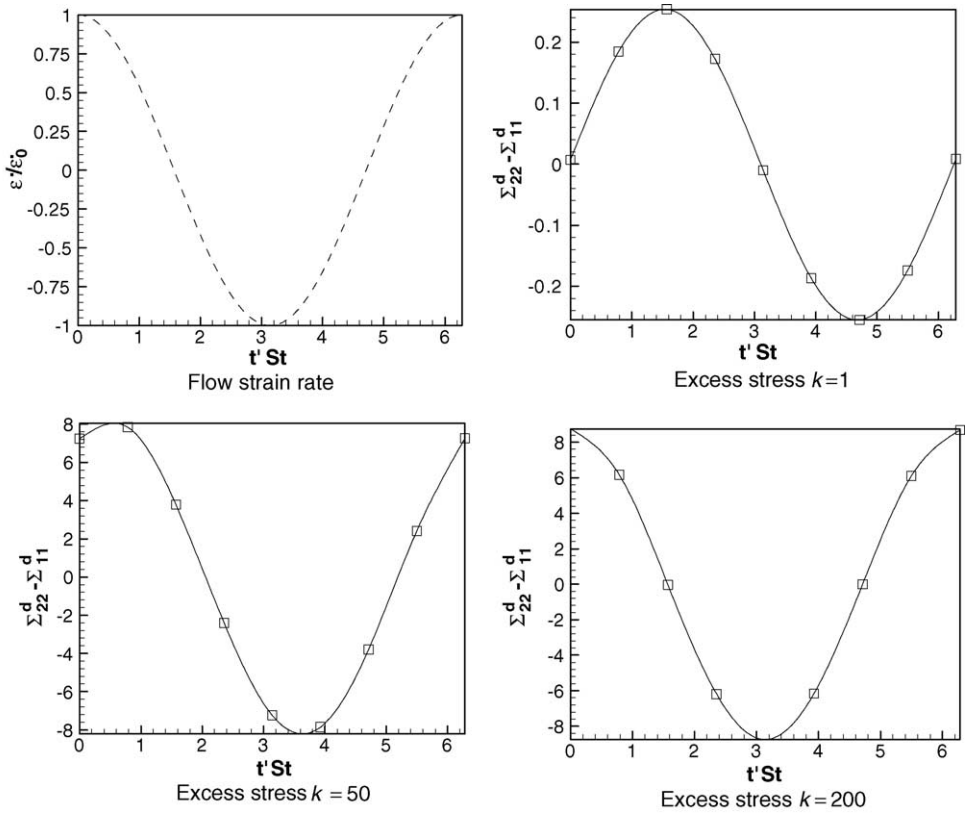

Fig. 8. Variation of flow strain rate (top left) and one-drop excess stress difference $\Sigma_{22}^{\mathrm{d}} - \Sigma_{11}^{\mathrm{d}}$ (others), during one period of steady oscillation; $St = 4\pi$, $Re = 0.1$.

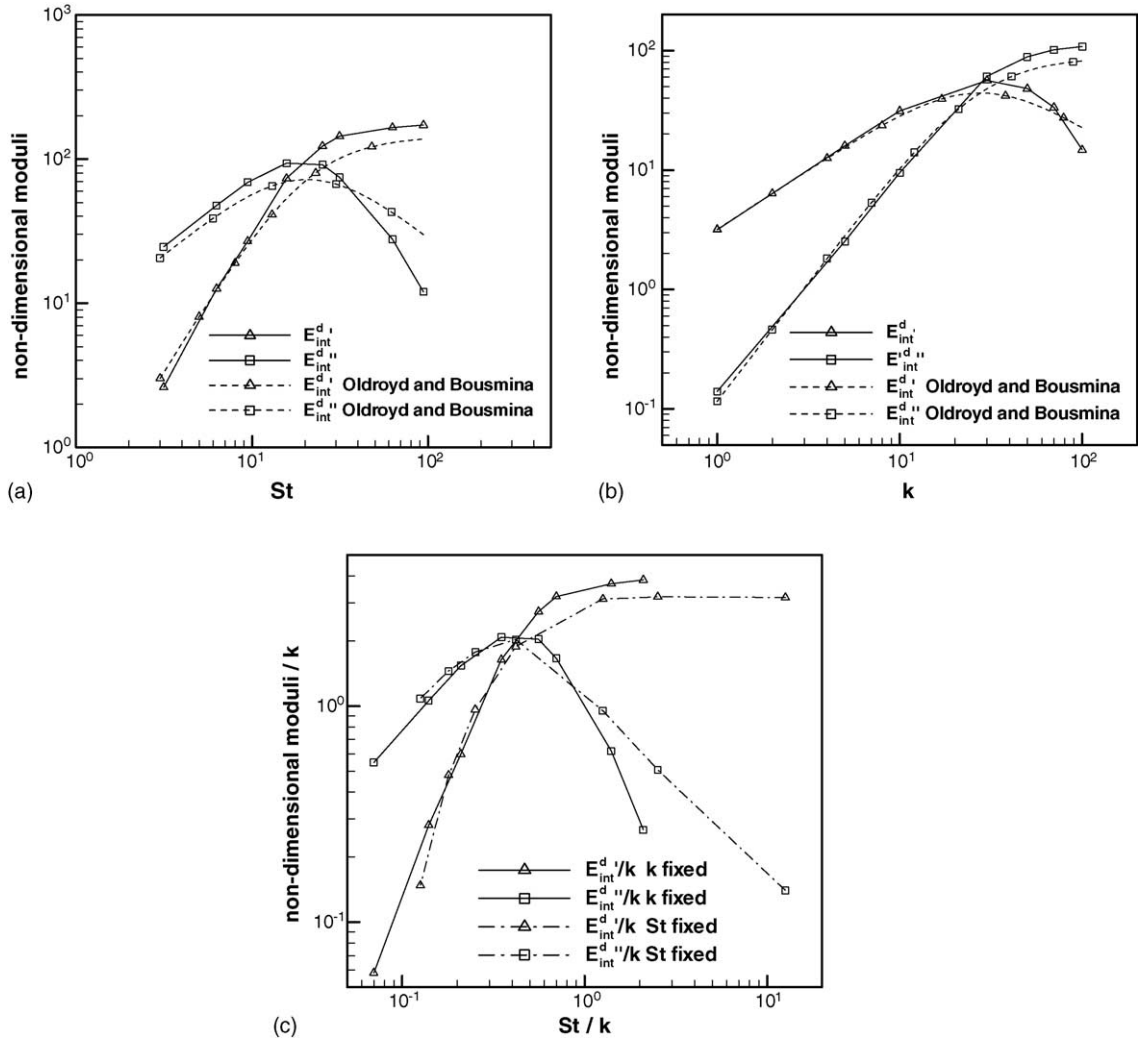

Fig. 9. Non-dimensional one-drop extensional moduli vs. St at $k = 45$ (a), vs. k at $St = 4\pi$ (b), and vs. St/k (c) along with Oldroyd's and Bousmina's models.

nificant, and lead to deviation from the Stokes-regime predictions.

In Fig. 9b, we plot interfacial moduli versus inverse capillary number k. The results match analytical prediction. For small interfacial tension, δ approaches zero, so that $E_{\text{int}}^{\text{d}''}$ approaches zero much faster than $E_{\text{int}}^{\text{d}'}$. As interfacial tension increases, δ increases such that the curve of $E_{\text{int}}^{\text{d}'}$ and $E_{\text{int}}^{\text{d}''}$ cross over. At high interfacial tension, δ approaches $\pi/2$ and $E_{\text{int}}^{\text{d}''}$ is much larger than $E_{\text{int}}^{\text{d}'}$. The analytical results (17) and (20) predict $E_{\text{int}}^{\text{d}'} \to 0$, and $E_{\text{int}}^{\text{d}''} \to 7St = 28\pi$ as $k \to \infty$. The behavior is in conformity with Fig. 8, where we saw that when the drop behaves like a viscous system at low interfacial tension, the emulsion interfacial stress is elastic, and vice versa.

In fact, the effects of variation in interfacial tension and frequency can be better understood by noting that the dynamics is governed by a competition between the relaxation time scale $\tau_0 \sim \mu R/\Gamma$ [see Eq. (13)] due to interfacial tension and the time period of oscillation ω^{-1} [46]. Accordingly, we plot in Fig. 9c the non-dimensional moduli shown in Fig. 9a and b further scaled by k as a function of St/k. Such a functional dependence is also predicted by the analytical result (20), noting that $\omega\tau_0 \sim St/k$. The plots for fixed k and fixed St match each other for smaller values of St/k. The discrepancy for larger St/k can be attributed to finite Reynolds number effects $\sim O(ReSt)$.

5. Summary

We have investigated extensional rheology of a dilute emulsion of drops using direct numerical simulation. The exact drop dynamics was computed using a front tracking method in an oscillating extensional flow. The drop shape is used to find the excess interfacial stress and interfacial moduli of the emulsion. The theory is linear in the volume fraction. The simulation results match the analytical predictions due to Oldroyd or Yu and Bousmina. The interfacial stress follows the evolving drop shape, particularly its phase giving rise to complex rheological response varying with frequency

and interfacial tension. As expected, the interfacial excess stress is predominantly viscous (elastic) for time period of oscillation much larger (smaller) than the relaxation time; the phenomenon is explained with the help of the drop dynamics. The drop–drop interaction neglected in the present analysis plays a significant role in a non-dilute emulsion. The methods used in this paper can be extended to investigate the rheology of concentrated emulsions, emulsions of viscoelastic drops [47,48] and emulsions at high drop inertia.

Acknowledgements

Financial support from Department of Mechanical Engineering, University of Delaware and University of Delaware Research Foundation is acknowledged. Authors also acknowledge suggested references from one anonymous reviewer.

References

[1] C.L. Tucker III, P. Moldenaers, Microstructural evolution in polymer blends, Ann. Rev. Fluid Mech. 34 (2002) 177–210.
[2] S. Wannaborworn, M.R. Mackley, Y. Renardy, Experimental observation and matching numerical simulation for the deformation and breakup of immiscible drops in oscillatory shear, J. Rheol. 46 (5) (2002) 1279–1293.
[3] R. Cavallo, S. Guido, M. Simeone, Drop deformation under small-amplitude oscillatory shear flow, Rheol. Acta 42 (2003) 1–9.
[4] W. Yu, M. Bousmina, Modeling of oscillatory shear flow of emulsions under small and large deformation fields, J. Rheol. 46 (6) (2002) 1401–1418.
[5] W. Yu, M. Bousmina, M. Grmela, J. Palierne, C. Zhou, Quantitative relationship between rheology and morphology in emulsions, J. Rheol. 46 (6) (2002) 1381–1399.
[6] B.J. Bentley, L.G. Leal, An experimental investigation of drop deformation and breakup in steady, two-dimensional linear flows, J. Fluid Mech. 167 (1986) 241–283.
[7] G.I. Taylor, The formation of emulsions in definable fields of flow, Proc. R. Soc. A 146 (1934) 501–523.
[8] R.G. Cox, The deformation of a drop in general time-dependent fluid flow, J. Fluid Mech. 37 (1969) 601–623.
[9] N.A. Frankel, A. Acrivos, The constitutive equations for a dilute emulsion, J. Fluid Mech. 44 (1970) 65–78.
[10] D. Barthes-Biesel, A. Acrivos, The rheology of suspensions and its relation to phenomenological theories for non-Newtonian fluids, Int. J. Multiphase Flow 1 (1973) 1–24.
[11] J.M. Rallison, Note on the time-dependent deformation of a viscous drop which is almost spherical, J. Fluid Mech. 98 (1980) 625–633.
[12] A. Acrivos, T.S. Lo, Deformation and breakup of a single slender drop in an extensional flow, J. Fluid Mech. 86 (1978) 641–672.
[13] E.J. Hinch, A. Acrivos, Long slender drops in a simple shear flow, J. Fluid Mech. 98 (1980) 305–328.
[14] D.V. Khakhar, J.M. Ottino, Deformation and breakup of slender drops in linear flows, J. Fluid Mech. 166 (1986) 185–265.
[15] H.A. Stone, Dynamics of drop deformation and breakup in viscous fluids, Ann. Rev. Fluid Dyn. 26 (1994) 65–102.
[16] M. Doi, T. Ohta, Dynamics and rheology of complex interfaces, Int. J. Chem. Phys. 95 (1991) 1242–1248.
[17] G.K. Batchelor, The stress system in a suspension of force-free particles, J. Fluid Mech. 41 (3) (1970) 45–570.
[18] J. Mellema, M.W.M. Willemse, Effective viscosity of dispersions approached by a statistical continuum method, Physica A 122A (1983) 286–312.
[19] A. Onuki, Viscosity enhancement by domains in phase-separating fluids near the critical points: proposal of critical rheology, Phys. Rev. A 35 (12) (1987) 5149–5155.
[20] A.S. Almusallam, R.G. Larson, M.J. Solomon, Comprehensive constitutive model for immiscible blends of Newtonian polymers, J. Rheol. 48 (2) (2004) 319–384.
[21] H.M. Lee, O.O. Park, Rheology and dynamics of immiscible polymer blends, J. Rheol. 38 (5) (1994) 1405–1425.
[22] G.W.M. Peters, S. Hansen, H.E.H. Meijer, Constitutive modeling of dispersive mixtures, J. Rheol. 45 (2001) 659–689.
[23] P.L. Maffettone, M. Minale, Equations of change for ellipsoidal drops in viscous flow, J. Non-Newtonian Fluid Mech. 78 (1998) 227–241.
[24] S. Guido, M. Villone, Three-dimensional shape of a drop under simple shear flow, J. Rheol. 42 (2) (1998) 395–415.
[25] Y.T. Hu, A. Lips, Transient and steady state three-dimensional drop shapes and dimensions under planar extensional flow, J. Rheol. 47 (2) (2003) 349–369.
[26] T. Jansseune, J. Mewis, P. Moldenaers, M. Minale, P.L. Maffettone, Rheology and rheological morphology determination in immiscible two-phase polymer model blends, J. Non-Newtonian Fluid Mech. 93 (2000) 153–165.
[27] T. Jansseune, I. Vinckier, P. Moldenaers, J. Mewis, Transient stresses in immiscible model polymer blends during start-up flows, J. Non-Newtonian Fluid Mech. 99 (2001) 167–181.
[28] E.D. Wetzel, C.L. Tucker III, Area tensors for modeling microstructure during laminar liquid–liquid mixing, Int. J. Multiphase Flow 25 (1999) 35–61.
[29] E.D. Wetzel, C.L. Tucker III, Droplet deformation in dispersions with unequal viscosities and zero interfacial tension, J. Fluid Mech. 426 (2001) 199–228.
[30] N.E. Jackson, C.L. Tucker III, A model for large deformation of an ellipsoidal droplet with interfacial tension, J. Rheol. 47 (3) (2003) 659–682.
[31] Y. Wu, A.Z. Zinchenko, R.H. Davis, Ellipsoidal model for deformable drops and application to non-Newtonian emulsion flow, J. Non-Newtonian Fluid Mech. 102 (2002) 281–298.
[32] W. Yu, M. Bousmina, Ellipsoidal model for droplet deformation in emulsions, J. Rheol. 47 (4) (2003) 1011–1039.
[33] M.R. Kennedy, C. Pozrikidis, R. Skalak, Motion and deformation of liquid drops and the rheology of dilute emulsions in simple shear flow, Comput. Fluids 23 (1994) 251–278.
[34] V. Cristini, C.W. Macosko, T. Jansseune, A note on transient stress calculation via numerical simulations, J. Non-Newtonian Fluid Mech. 105 (2002) 177–187.
[35] M. Loewenberg, E.J. Hinch, Numerical simulation of a concentrated emulsion in shear flow, J. Fluid Mech. 321 (1996) 395–419.
[36] A.Z. Zinchenko, R.H. Davis, Shear flow of highly concentrated emulsions of deformable drops by numerical simulations, J. Fluid Mech. 455 (2002) 21–62.
[37] R. Scardovelli, S. Zaleski, Direct numerical simulation of free-surface and interfacial flow, Ann. Rev. Fluid Dyn. 31 (1999) 567–603.
[38] J.A. Sethian, P. Smereca, Level set methods for fluid interfaces, Ann. Rev. Fluid Dyn. 35 (2003) 341–372.
[39] G. Tryggvason, B. Bunner, O. Ebrat, W. Taubar, Computation of multiphase flows by a finite difference front tracking method. I. Multi-fluid flows, 29th Computational Fluid Dynamics Lecture Series 1998–03, Von Karman Institute of Fluid Dynamics, 1998.
[40] K. Sarkar, W.R. Schowalter, Deformation of a two-dimensional drop at non-zero Reynolds number in time-periodic extensional flows: numerical simulation, J. Fluid Mech. 436 (2001) 177–206.

[41] K. Sarkar, W.R. Schowalter, Deformation of a two-dimensional viscous drop in time-periodic extensional flows: analytical treatment, J. Fluid Mech. 436 (2001) 207–230.
[42] K. Sarkar, W.R. Schowalter, Deformation of a two-dimensional viscoelastic drop at non-zero Reynolds number in time-periodic extensional flows, J. Non-Newtonian Fluid Mech. 95 (2000) 315–342.
[43] X. Li, K. Sarkar, Drop dynamics in an oscillating extensional flow at finite Reynolds numbers, Phys. Fluids 17, 027103 (2005).
[44] J.G. Oldroyd, The elastic and viscous properties of emulsions and suspensions, Proc. R. Soc. A218 (1953) 122–132.
[45] J.G. Oldroyd, The effect of interfacial stabilizing films on the elastic and viscous properties of emulsions, Proc. R. Soc. A232 (1955) 567–577.
[46] M. Bousmina, Effect of interfacial tension on linear viscoelastic behavior of immiscible polymer blends, Rheol. Acta 38 (1999) 251–254.
[47] W. Yu, M. Bousmina, C. Zhou, C.L. Tucker, Theory for drop deformation in viscoelastic systems, J. Rheol. 48 (2) (2004) 417–438.
[48] P.L. Maffettone, F. Greco, Ellipsoidal drop model for single drop dynamics with non-Newtonian fluids, J. Rheol. 48 (1) (2004) 83–100.